J Chem Technol Biotechnol 78:314–320 (online: 2003)
DOI: 10.1002/jctb.778

Performance enhancement of a chemical reactor utilizing flow instability†

Mohammad F Kabir and Ajay K Ray*
Department of Chemical and Environmental Engineering, National University of Singapore, 10 Kent Ridge Crescent, Singapore 119260

Abstract: A detailed analysis has been performed for a heterogeneous photocatalytic Taylor vortex reactor that uses flow instability to recirculate fluid continually from the vicinity of the rotating inner cylindrical surface to the stationary outer cylindrical surface of an annulus. A comprehensive time accurate computation shows the different stages of flow evolution and the effects of finite length of the reactor in creating eddies, the overall effects of which shows very high efficiency of photocatalytic conversion. The physical arrangement considered is such that pollutant degradation is maximized by a combination of the Controlled Periodic Illumination (CPI) effect and the motion of fluid particles in a specific regime of centrifugal instability.

Keywords: photocatalytic reactor; simulation; Taylor–Couette flow; multiphase reactions; multiphase reactors

NOTATION

AR	Aspect ratio (dimensionloss)
d	Annular gap (m)
L	Length (m)
r	Radius (m); radial direction (m)
Re	Reynolds number (dimensionloss)
t	Time (s)
t^*	Dimensionless time $\equiv t\ (\Omega\ r_i)/d$
Ta	Taylor number (dimensionless)
V	Velocity (m s^{-1})
Y	Axial direction (m)
δ	Boundary layer thickness (m)
κ	Illuminated catalyst density ($m^2\,m^{-3}$)
υ	Kinematic viscosity ($m^2\,s^{-1}$)
ρ	Density ($kg\,m^{-3}$)
Ω	Rotation rate (rad s^{-1})

Subscripts

i	Inner
o	Outer

INTRODUCTION

Heterogeneous photocatalysis is one of the advanced oxidation technologies for air and water purification treatment and is documented in various references.[1–5] However, practical application of this technology is not fully exploited due to various limitations.[6] The scale-up of fixed-bed photocatalytic reactors has been severely limited as reactor configurations have not been able to address the issue of mass transfer of pollutants to the catalyst surface. Earlier experimental studies of our group on catalyst-coated tube bundles,[7] novel immersion type lamps,[8] and rotating tube bundles revealed that photocatalytic reaction is mainly diffusion (mass-transfer) controlled. The reaction occurs at the fluid–catalyst interface and, in most cases, the overall rate of reaction is limited to mass transport of the pollutant to the catalyst surface. In our earlier studies, we have enhanced mass transfer by increasing mixing of fluids through turbulence and introduction of baffles.[9] In this work, a new reactor is developed that uses flow instability to increase reaction yield throughout the reactor volume.

Centrifugal instability of rotating Couette flows

The laminar flow confined within the annulus region between two co-axial cylinders with the inner one differentially rotating with respect to the outer suffers centrifugal instability depending on the geometry and rotation rates. The first experimental reporting was by Taylor,[10] who showed an inviscid rotating flow to be unstable, if the energy of rotation associated with a fluid particle decreases radially outward. Under such unstable configuration one notices the appearance of circumferential toroidal vortices in between the two cylinders, known as Taylor–Couette vortices. These vortices evolve due to the adverse gradient of angular momentum that creates potential unstable arrangement of flow. Such an unstable condition arises naturally if the outer cylinder is held stationary while the inner cylinder is rotated at a sufficiently high rotation rate, an arrangement considered for the

* Correspondence to: Ajay K Ray, Department of Chemical and Environmental Engineering, National University of Singapore, 10 Kent Ridge Crescent, Singapore 119260
E-mail: cheakr@nus.edu.sg
† Paper presented at the Process Innovation and Process Intensification Conference, 8–13 September 2002, Edinburgh, UK
(*Received 15 April 2002; accepted 29 September 2002*)

present application. A schematic of such a Taylor vortex reactor (TVR) is shown in Fig 1.

Sczechowski *et al*[11] have used semiconductor photocatalyst particles as a slurry in the fluid within the annulus. They have found that despite the photocatalyst being dispersed in the fluid, the useful reaction takes place only periodically when the fluid is in contact with the illuminated inner cylinder surface. This is the principle of Controlled Periodic Illumination (CPI). It was reported that the photo-efficiency increases three-fold when the reactant is illuminated for less than 150 ms, and it stayed in the dark for more than 1 s. The maximum photo-efficiency achieved by them was 30% at 300 rpm of the inner cylinder when a 10 g dm^{-3} loading of TiO_2 was used. The major problem of achieving higher photo-efficiency (apart from the CPI effect) is related to the transport of purified fluid from the vicinity of the catalyst. Furthermore, there exists the additional problem of separation of sub-micron size catalyst particles after the purification stage. Moreover, the working fluid is optically dense and, therefore, the light penetration depth is restricted to a distance that is of the order of the boundary layer thickness of the inner cylinder. In view of all these factors, in the current work a TVR of similar geometry has been considered, but instead of a slurry-type reactor, the photocatalyst was assumed to be immobilized (fixed) on the outer surface of the inner cylinder, and a fluorescent lamp illuminates the inner cylinder. Thus, one can use a very low level of catalyst loading and simultaneously eliminate the process of separation of catalyst particles after the purification stage. The enhanced purification has been obtained by utilizing fluid dynamical instability associated with centrifugal instability in the cylindrical annular geometry. It is, therefore, essential to focus on the twin aspects, photocatalysis and centrifugal instability, in an annular cylindrical geometry.

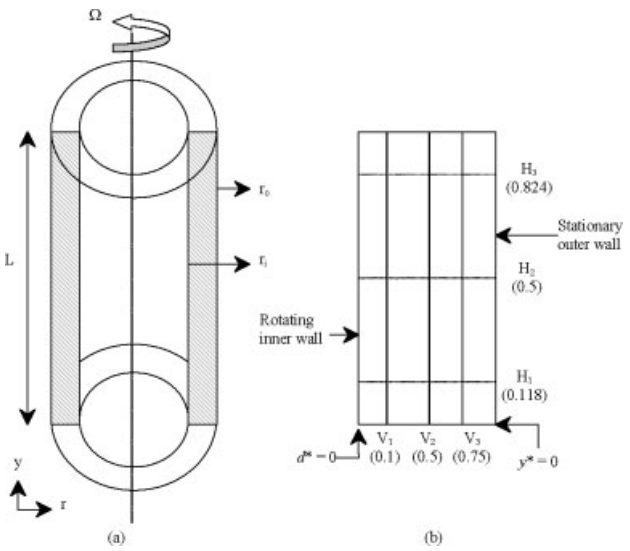

Figure 1. (a) Schematic diagram of the Taylor vortex reactor, and (b) location of the observation stations in the annular region to analyze flow behavior. $d^*=0$ (rotating inner cylinder), $d^*=1$ (stationary outer wall), $y^*=0$ (bottom), $y^*=1$ (top).

By assuming the annular gap, $d=(r_o-r_i)$, as being small compared with the inner cylinder radius (r_i), where r_o is the outer cylinder radius, it has been shown by Taylor[10] that stability is dependent only on the ratio of the rotation rate of the outer cylinder to the rotation rate of the inner cylinder (Ω_o/Ω_i), and a single parameter, called the Taylor number, *Ta*, which describes the influence of rotation about a vertical axis on a convective system and can be defined as follows:

$$Ta = \frac{r_i d^3 \lfloor \Omega_i^2 - \Omega_o^2 \rfloor}{\upsilon^2} \qquad (1)$$

The non-wavy vortex flow is seen to appear as a consequence of primary instability as given by appropriate non-dimensional numbers like the Taylor number and Reynolds number. When the aspect ratio of the geometry is very large, the primary instability in the form of the appearance of Taylor vortices occurs at $Ta_{crit} \approx 1708$. When the Reynolds number (defined here in terms of the gap width as the length scale and the surface velocity on the inner cylinder surface as the velocity scale, ie $Re = r_i \Omega d/\upsilon$) is increased, one sees the wavy vortex flow and, with time, the annulus is filled with pairs of counter-rotating vortices. The boundary layer also oscillates periodically between almost zero thickness to a maximum in between the counter-rotating vortex pair, where the two shear layers approaching each other spew out a jet of fluid towards the outer wall. In their motion around the toroidal vortices the fluid particles come periodically in contact with the inner surface where the catalyst is immobilized, and in the presence of light the catalyst is activated and as a result the redox reaction takes place. The residence time in the illuminated region is thus a function of the angular velocity of the recirculating vortex as well as the size of the vortex. The latter, once again, depends on the gap size and the number of vortices formed in a given length of the reactor. A good design of the reactor would be one that moves the particles on the time scales established for the optimal CPI effect. It should also be noted that when the outer cylinder is stationary:

$$Ta = Re^2 \times (d/r_i).$$

It has been reported[12] that the transfer of fluid particles between adjacent vortices occurs in a cyclic fashion as a particular vortex gains fluid from adjacent vortices. The vortices became stronger and the outflow between pairs of vortices becomes jet-like. It has also been reported that the degree of transfer of fluid is greater at $Re = 253$ than at either higher or lower Reynolds numbers. In addition to flow into and out of adjacent vortices taking place periodically, the individual vortex centers also move both axially and radially in a cyclic fashion so that while one vortex grows in size, the two adjacent vortices become smaller, and

vice versa. Once again the maximum departure in the radial direction is a strong function of Reynolds number and is found to be maximum for $Re = 253$. This aspect of the flow is important, because traditionally it is assumed that the vortex pairs in Taylor–Couette vortices are independent of each other and of same size, and it is customary to treat this as plug flow. This is particularly significant from the point of view of the present application. If indeed there is significant mass transfer between adjacent vortex pairs, then that can be used for additional benefit for the performance enhancement of the reactor. It is for these reasons that it was decided to investigate a geometry that corresponds to this optimum Reynolds number. However, to avoid computing for long times, and also for practical usefulness, the flow establishment is considered to be in an impulsive fashion.

COMPUTATIONAL DETAILS

In computing the flow the three-dimensional Navier–Stokes equation is solved in primitive formulation by using the commercial software FLUENT®. This is found to be adequate as the flow considered is laminar, and would thus be computed without the need for resolving large ranges of wave numbers and circular frequencies. In solving the governing equations, no simplification is made regarding symmetry and reflection of the solution. Also, the solution that is sought for is the time-accurate solution and *a priori* steady state solution is not assumed. The geometric dimensions chosen for the reactor are identical to those of the value chosen in Werely and Lueptow[13] and are given in Table 1. The model pollutant considered in this work is phenol, and the starting concentration is taken as 100 ppm. Since this is a trace quantity, it is expected that the chemical reaction will not influence the fluid dynamic behavior of the system. To show this, two sets of computations were initiated from $t = 0$, one with the chemical reaction, while in the other only the fluid flow was computed and the results compared found to be identical. The rate expression for photocatalytic degradation for phenol used in this study is given by:[3]

$$R = -\frac{dC_S}{dt} = k_0 \exp\left[-\frac{E}{RT}\right] I^{\beta}\left[\frac{K_{O_2} p_{O_2}}{1 + K_{O_2} p_{O_2}}\right]\left[\frac{K_S C_S}{1 + K_S C_S}\right] \quad (2)$$

where: $k_0 = 1.19 \times 10^{-4}\,\text{mol m}^{-2}\text{s}^{-1}$, $E = 11.80\,\text{kJ mol}^{-1}$, $\beta = 0.82$, $K_{O_2} = 12.71\,\text{atm}^{-1}$, $K_S = 4.26\,\text{mM}^{-1}$. However, it should be noted that the overall photocatalytic degradation rate is a function of numerous other parameters such as wavelength and angle of incidence of light, catalyst layer thickness, pH, presence of other ions, and external and internal mass transfer.[1–5] Therefore, the photocatalytic reaction rate can vary an order of magnitude depending on the various parameter values. The amount of catalyst coating is assumed[7,8] to be $3 \times 10^{-3}\,\text{kg m}^{-2}$.

Table 1. Geometric dimensions of the reactor configurations considered

Length, L(m)	0.4245
Inner radius, r_i (m)	0.0434
Outer radius, r_o (m)	0.0523
Annular gap, d (m)	0.0089
Aspect ratio, L/d (dimensionless)	47.70
Rotation speed, Ω (rad s^{-1}) (rpm)	0.655 (6.25)
Volume of liquid treated, V_L(m^3)	1.136×10^{-3}
Illuminated catalyst density, κ(m^{-1})	102
Reynolds number, *Re* (dimensionless)	253
Taylor number, *Ta* (dimensionless)	13 126

For generating grids within the annulus region of the geometry, every edge in three directions was defined with certain nodes. There are high shear regions near the inner cylinder wall, the outer cylinder wall and the end cap regions. Therefore, axial and radial derivatives of all physical variables across such layers would be larger than in the azimuthal direction, and consequently, more grid points are taken in axial and radial directions compared with azimuthal direction. In order to incorporate these, grid points are taken more clustered in two ends and next to inner and outer wall. To enhance the direct mapping of grid from upper wall to bottom wall, the total geometry is separated into two volumes by a brick. Two interior planes were created by this process within the annular space that was used to analyze our results at the time of post processing. To get the instability pattern of flow in annular area, both the finer grid and coarser grid were chosen to analyze grid dependency of results. Grid points along the three directions were taken as follows: $r \times \theta \times h = 200 \times 60 \times 150$ in the fine-grid case and $100 \times 40 \times 75$ in the coarse-grid case. FLUENT preprocessor GAMBIT® 1.1 was used to create the geometry and generate grids for both cases. For the finer grid the mesh volume is 1.8 million with total of 1 821 060 nodes and total elements are once again 1.8 million. Its creation requires a total of 393.66 CPUs with 431.2 MB memory. For the coarser grid there are 0.3 million cells, 907 000 total quadrilateral faces (3000 inner wall faces, 11 000 outer wall spaces, 15 000 interior plane faces and 878 000 rest of interior plane faces). The total number of nodes is 307 040.

The present set of computation of Navier–Stokes equation for Taylor–Couette geometry is expensive. For the finer grid case, the random access memory (RAM) requirement is 1.3 Gigabytes, which demands a large computing machine. The one with reaction (flow plus reaction) was carried out on a 1.5 Gb RAM Windows NT workstation and the other, without reaction, was performed on a mainframe supercomputer (SGI origin 2000). For the coarse grid, the CPU requirement is considerably less as the number of grids was one-sixth of the finer one.

Since the flow inside the reactor is driven by the rotating inner cylinder and the rotation rates are low, it is quite adequate to consider the flow to be incompressible and solve the governing Navier–Stokes

equation in primitive variable form as:

$$\frac{\partial \vec{V}}{\partial t} + (\vec{V} \cdot \nabla)\vec{V} = -\frac{1}{\rho}\nabla p + v\nabla^2 \vec{V} \qquad (3)$$

and

$$\nabla \cdot \vec{V} = 0 \qquad (4)$$

Furthermore, isothermal condition can be assumed for both the flow evolution and chemical reaction calculations since the pollutant being oxidized into other products is present in trace amounts, and the heat of reaction in photocatalytic reactions is usually negligible.[3]

The boundary conditions that are applied on the inner and outer cylindrical surface correspond to no-slip conditions. The end caps are considered a part of the outer cylinder and hence are stationary. The following boundary conditions are used for the numerical simulations. With reference to Fig 1, on the inner cylinder surface, $r = r_i$:

$$V_r = V_y = 0 \text{ and } V_\theta = \Omega_i r_i \qquad (5a)$$

where $\Omega_i(t)$ is the instantaneous rotation rate of the inner cylinder. On the outer cylinder ($r = r_o$) and the end-caps ($y = 0$ and L):

$$V_r = V_y = V_\theta = 0 \qquad (5b)$$

Since the simulation is for the impulsive start of the rotation rate of the inner cylinder,

$$t \leqslant 0: \quad \Omega_i(t) = 0 \qquad (6a)$$

$$t > 0: \quad \Omega_i(t) = \Omega \qquad (6b)$$

The initial concentration of phenol is taken as 100 ppm while the initial mass fraction of O_2 is taken to be equal to 0.0006, which is twice the stoichiometric requirement for the reaction given by:

$$C_6H_5OH + 7\ O_2 \rightarrow 6CO_2 + 3H_2O \qquad (7)$$

Equations (3) and (4) are solved subject to the boundary conditions and initial conditions defined in eqns (5) and (6) within the annulus between the cylinders, as shown in Fig 1. The solver is based on solving eqns (3) and (4) in a sequential manner by a control volume based technique using the following three steps. Firstly, the computing domain was discretized into discrete control volume using a computational grid. The governing equations were time advanced in integral form for each computational cell to yield algebraic equations for the discrete dependent variables, such as velocity components, pressure and conserved scalars. Finally, the discrete equations were linearized into a set of algebraic equations, which were solved to yield updated variables. For the discretization process, the familiar QUICK scheme was used for the momentum and species equations, as this is a higher-order accurate scheme with minimum numerical dissipation that is implicit with the discretization.

RESULTS AND DISCUSSION

The contour plots of axial and radial velocity component along the bottom half of the reactor length are shown in Fig 2. One can notice the variable sizes of vortices formed along the length of the reactor, and specifically the smaller vortices near the end-caps. In Fig 3, the detailed velocity vectors are shown for the top half of the reactor ($y^* = 0.5$–1.0) in a given y–r plane at $t = 330$ s when steady state is almost reached. The segment between 50% and 70% of the reactor height is shown on the left, the segment between 70% and 85% is shown in the middle while the remaining segment of the top half is shown on the right. One can see weak vortices forming near the upper part of the left segment. There are regions along the height where one can see a jet-like flow starting from the inner wall

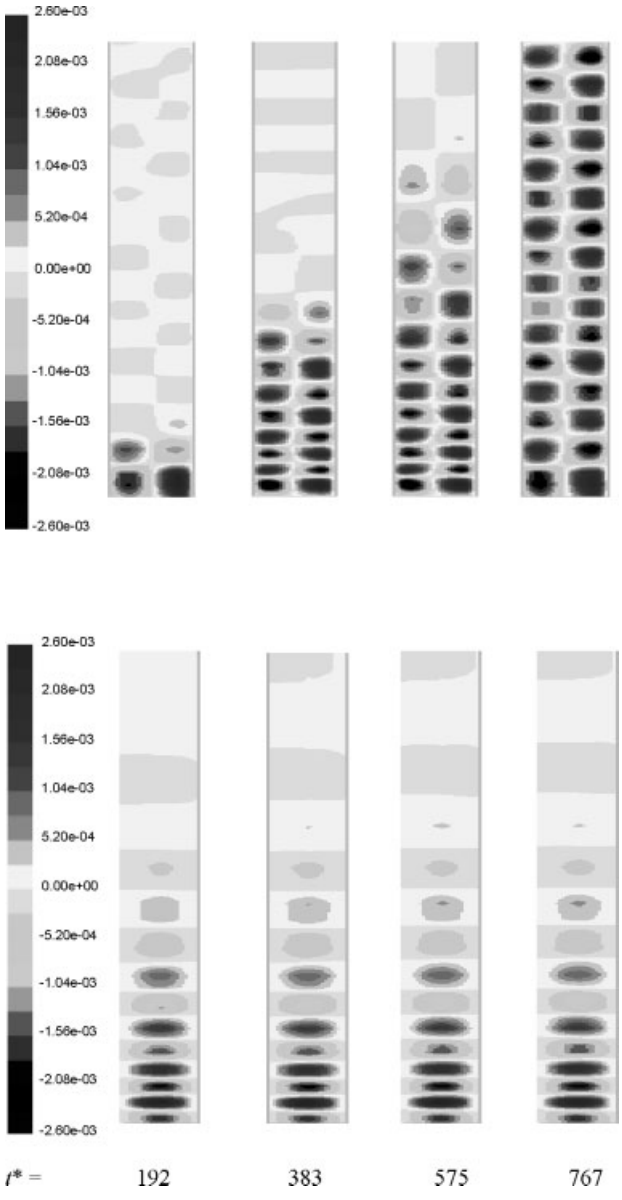

Figure 2. Flow evolution is shown with axial and radial velocity contour in interior plane at various times for the bottom half of the reactor length. Right boundary indicates rotating inner wall and left hand side indicates stationary outer wall. Top figure shows axial velocity contours while the bottom figure shows radial velocity contours.

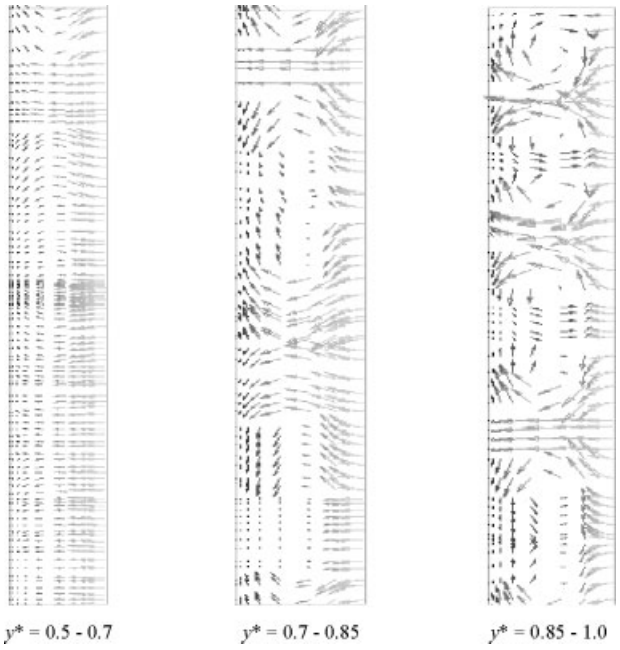

Figure 3. Velocity vectors shown in radial plane respectively between $y^*=0.5$–0.7, $y^*=0.7$–0.85 and $y^*=0.85$–1.0 at $t=330$s. Right-hand side indicates rotating inner wall ($d^*=0$).

moving towards the outer wall due to centrifugal action. In the segment between $y^*=0.7$–0.85, significant mixing of fluid is noticeable due to the formation of coherent vortices in part of the reactor. Once again one can see the jet-like flow from the inner to the outer cylinder, although the trajectories of the fluid particles are not strictly straight. Moreover, there are no visible wall shear layers forming on the inner wall. In the segment between $y^*=0.85$–1.0, the velocity vectors clearly show re-circulating rolls, although the axial lengths vary significantly due to end-wall effects. Also in this segment, apart from the jet-like regions, one can as well see small axial regions where a flow is established from the outer to the inner wall side. However, this cannot cover the entire radial gap because of centrifugal force acting on fluid particles near the inner wall. The velocity vectors inside the re-circulating eddies show time-dependent behavior, though it is not so pronounced near the middle section of the reactor where the eddies are either very weak or not formed. All of these unsteady events would lead to an increase of mass exchange between adjacent fluid cells.

In Fig 4 the axial velocity as a function of radial distance is plotted for various time instants at the observation stations H_1, H_2 and H_3 of Fig 1(b). Since the middle section (H_2) is at the centre ($y^*=0.5$), there the axial velocity is smallest in magnitude as compared with the other two stations where the maximum velocity component is of the order 5–6% of the velocity scale. The results also indicate that the flow is not fully developed even at $t^*=767$, although the rate of change of flow quantities has decreased significantly. Similarly in Fig 5, the non-dimensional radial component of velocity is plotted in the annular

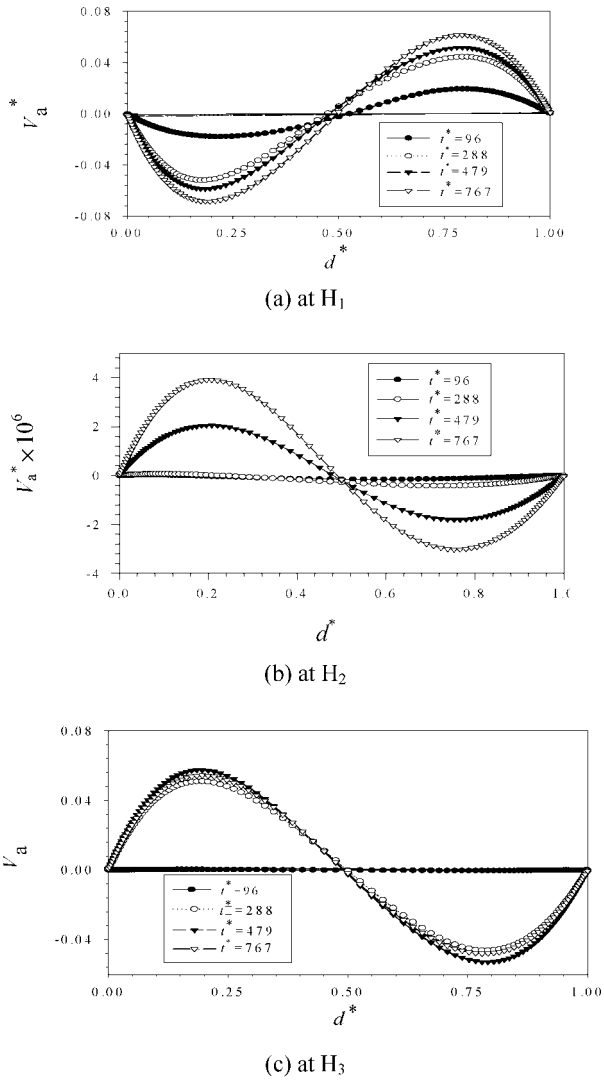

Figure 4. Change of dimensionless axial velocity (V_a^*) with dimensionless radial coordinate (d^*) at different axial locations (H_1–H_3) and dimensionless times.

gap at the three different heights at four different non-dimensional times. Once again at H_2, the magnitude of the velocity is the smallest. Figure 5(a), for H_1, indicates an inflow of fluid towards the inner cylinder for all the indicated times, while at H_3 for up to $t^*=575$ the fluid particles move towards the inner cylinder but at $t^*=767$ the fluid particles move towards the outer cylinder. For the mid-plane (H_2), the radial velocity components are two orders of magnitude smaller and the flow does not show the formation of Taylor–Couette vortices in the middle part of the reactor.

In Fig 6, the non-dimensional axial velocity is plotted along the axial direction at observation stations V_1, V_2 and V_3. At smaller times, the Taylor–Couette vortices are formed at the ends and as time progresses more and more of these are formed covering the middle part. Of specific interest is the plot of the axial velocities in the middle of the annulus at V_2. If indeed the vortices formed are like a plug flow then this velocity component along this line would have been

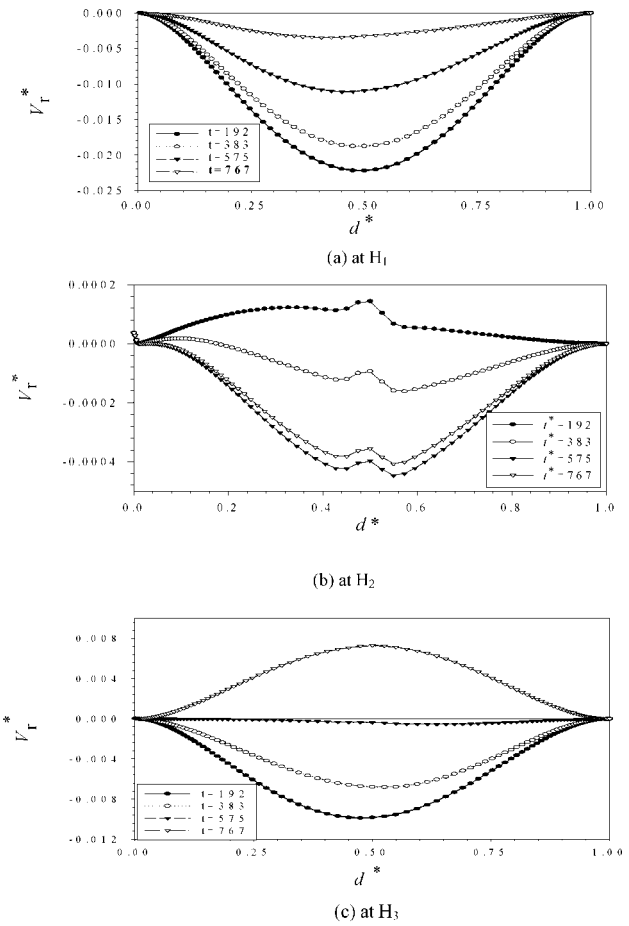

Figure 5. Change of dimensionless radial velocity (V_r*) at various annular gap locations (d*) for different locations (H_1–H_3) and dimensionless times (t*).

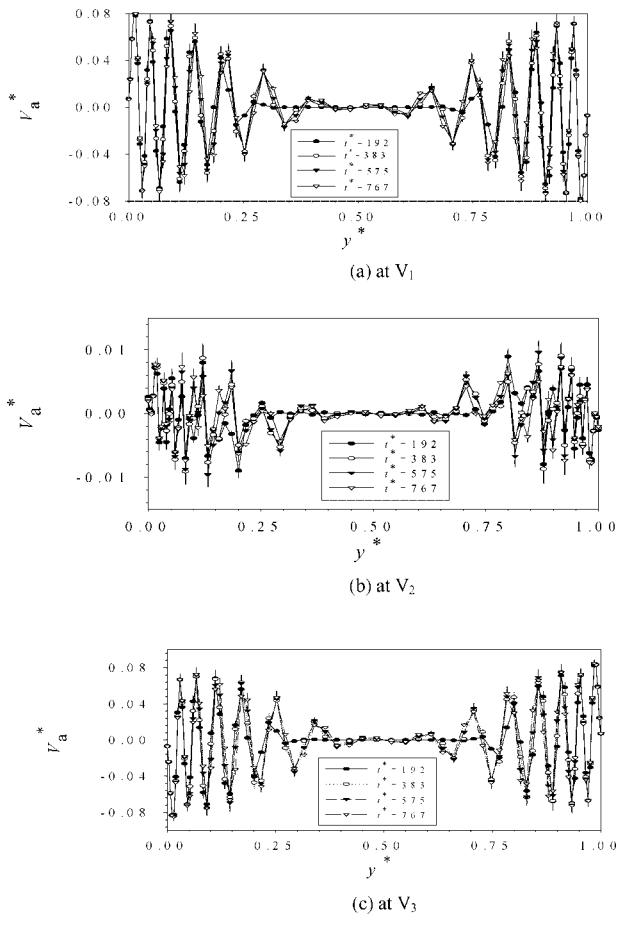

Figure 6. Change of dimensionless axial velocity (V_a*) at different locations (V_1–V_3) for different dimensionless positions of annular gap widths (d*) and times (t*).

zero. The very fact that the velocity component alternates in sign is indicative of the fact that the vortex centers not only execute axial waviness but also shows significant radial motion. This was also observed experimentally by Werely and Lueptow[13] who showed such motions for all Reynolds numbers between 131 and 1221. They reported large excursions of axial motions for low Reynolds numbers while maximum radial motion of vortex centers were observed for $Re = 253$. However, it has to be noted that in the present investigation the flow is started impulsively and not accelerated quasi-statically, and the flow is not completely fully developed. This aspect is clearly demonstrated in the contour plots of axial and radial velocity component along the bottom half of the reactor length shown in Fig 2. One can notice the variable sizes of vortices formed along the length of the reactor, and specifically the smaller vortices near the end-caps.

To analyze the performance of the TVR, phenol is considered as typical pollutant present in water with an initial concentration of 100 ppm. Pollutant degradation as integrated over the full reactor volume is shown as function of non-dimensional time in Fig 7. It is to be noted that after 210 s ($t^* = 671$) of operation, pollutant is degraded by about 57%. It clearly indicates the role of Taylor–Couette vortices in enhancing the rate of pollutant degradation. At early times the very rapid rate of degradation is due to the vortices that form at the fixed ends where strong recirculating zones causes rapid mass transfer from inner to outer cylinder and

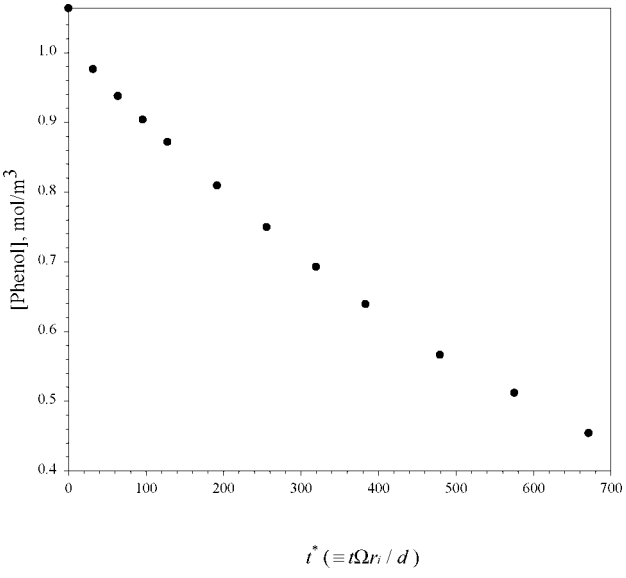

Figure 7. Photocatalytic degradation of phenol with time.

Table 2. Comparison of performance of Taylor vortex reactor (TVR) with that of a classical annular reactor (CAR) for photocatalytic degradation of phenol

	CAR[12]	*TVR*[a]
Volume of reactor (m^3)	3.48×10^{-3}	3.65×10^{-3}
Catalyst surface area (m^2)	0.18	0.116
ICD,[7,8] κ ($m^2 m^{-3}$)	69	102
Volume of liquid treated (m^3)	2.6×10^{-3}	1.136×10^{-3}
Electrical energy input (W)	400	100
Time for 50% conversion (s)	480	165
Efficiency[b] ($s^{-1} m^{-3} W^{-1}$)	0.0010	0.0267
% increase in efficiency	0	2570

[a] Efficiency is defined as 50% pollutant (phenol) converted per unit time (s) per unit reactor volume (m^3) per unit electrical energy input (W).

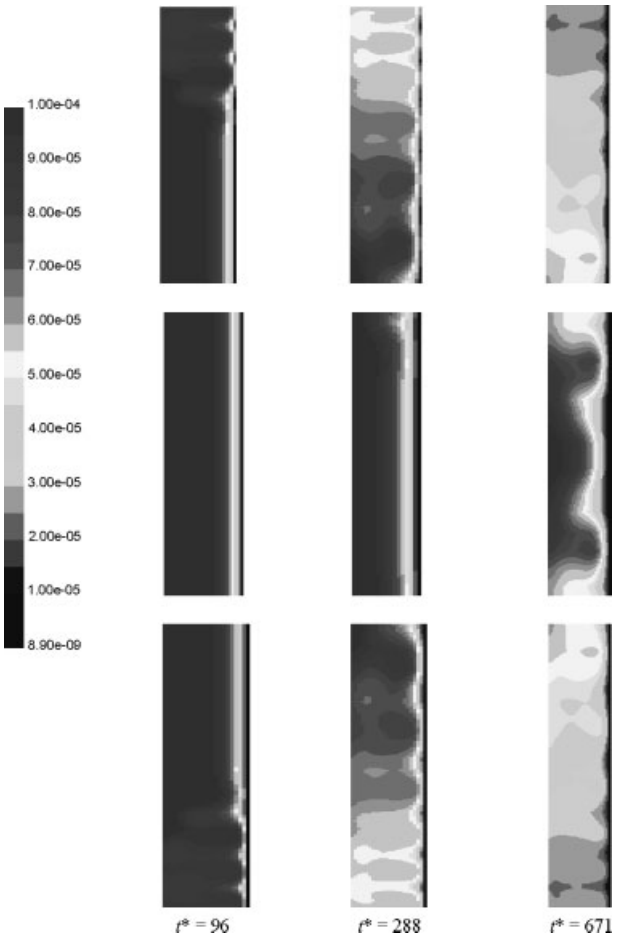

Figure 8. Contour plots of photocatalytic degradation of phenol with time. The scale of pollutant mass fraction is shown at the left of the figure [$1.0 \times 10^{-4} \equiv 1.064$ mo m^{-3} (100 ppm)]. The entire reactor length is divided into top 30%, middle 40% and bottom 30% respectively in the figure.

back. Later one can notice an almost constant pollutant degradation rate till $t^* = 671$ up to which the results are reported here. Table 2 compares the performance of a classical annular reactor (CAR)[12] with that of the TVR considered in this work. In Fig 8, the pollutant mass fraction contours are shown at different times. Close scrutiny of Fig 2, where it is seen that in the middle 40% of the length, the Taylor–Couette vortices are not well formed while well-developed vortices are present at either ends, explains the mass fraction contour plots of pollutant in Fig 8. This type of flow evolution directly influences the photocatalytic oxidation of pollutant and can be seen in Fig 8. The reaction takes place only in the shear layer of the inner cylinder where catalyst is present, and Taylor vortices are very efficient at enhancing the reaction by transporting the pollutant from the bulk to the catalyst surface. Hence, the pollutant is degraded very quickly as the vortex develops. Figures 7 and 8 also indicate the possibility of operating the reactor in the transient mode by periodic switching on and off the reactor since during the transient phases the reaction proceeds at a very rapid rate due to the vortices near the end walls.

REFERENCES

1 Ray AK and Beenackers AACM, Novel swirl-flow reactor for kinetic studies of semiconductor photocatalysis. *AIChE J* **43**:2571–2578 (1997).
2 Chen DW and Ray AK, Photodegradation kinetics of 4-nitrophenol in TiO_2 suspension. *Wat Res* **32**:3223–3243 (1998).
3 Chen DW and Ray AK, Photocatalytic kinetics of phenol and its derivatives over UV irradiated TiO_2. *Appl Catal B: Environ* **23**:143–157 (1999).
4 Chen DW, Li F and Ray AK, Effect of mass transfer and catalyst layer thickness on photocatalytic reaction. *AIChE J* **46**(5):1034–1045 (2000).
5 Chen DW and Ray AK, Removal of toxic metal ions from wastewater by semiconductor photocatalysis. *Chem Eng Sci* **56**(4):1561–1570 (2001).
6 Mukherjee PS and Ray AK, Major challenges in the design of a large-scale photocatalytic reactor for water treatment. *Chem Engg Technol* **22**:253–260 (1999).
7 Ray AK, Design, development and experimentation of a new photocatalytic reactor for water treatment. *Chem Eng Sci* **54**(16):3113–3125 (1999).
8 Ray AK and Beenackers AACM, Novel photocatalytic reactor for water purification. *AIChE J* **44**:477–483 (1998).
9 Periyathamby U and Ray AK, Computer simulation of a novel photocatalytic reactor using distributive computing. *Chem Eng Technol* **22**(10):881–888 (1999).
10 Taylor GI, Stability of a viscous liquid contained between two rotating cylinders. *Phil Trans R Soc* **A 223**:289–295 (1923).
11 Sczechowski JG, Koval CA and Noble RD, A Taylor vortex reactor for heterogeneous photocatalysis. *Chem Engg Sci* **50**(20):3163–3170 (1995).
12 Assink JW, Koster TPM and Slaager JM, Fotokatalytische oxydatie voor afvalwaterbehandeling, Report Reference No 93–137, Instituut voor Milieu en Energie-technologie (TNO), Apeldoorn, The Netherlands (1993).
13 Werely ST and Lueptow RM, Spatio-temporal character of non-wavy and wavy Taylor Couette flow. *J Fluid Mech* **364**:59–66 (1998).